CrossMark

# Influence of In-doping on microstructure, optical and electrical properties of sol–gel derived CdO thin films

I. Ben Miled[1,2] · M. Jlassi[3] · I. Sta[1] · M. Dhaouadi[1,2] · M. Hajji[4] · G. Mousdis[5] · M. Kompitsas[5] · H. Ezzaouia[1]

## Abstract

Cadmium oxide thin films have been prepared on glass substrates by the sol–gel (SG) spin-coating technique. The structural, optical and electrical properties of the prepared films were studied as a function of the thicknesses. The results show that the optimum thickness for preparation of CdO films with high optical transparency and low resistivity is 211 nm. By using this optimized thicknesses and the same experimental conditions, transparent indium-doped cadmium oxide (In–CdO) thin films were deposited and annealed at 450 °C. Transparent and conducting In–CdO thin films for various concentrations of indium (1, 3 and 5 wt%), were prepared using the SG method. The electrical, optical and structural properties of these In–CdO films were investigated using different techniques, such as Hall measurements, optical transmission and X-ray diffraction (XRD). XRD patterns show that the films are polycrystalline. The structural analysis shows that all the samples have a cubic structure. Field emission scanning electron microscopy analysis reveals that the average grain size and surface morphology of CdO films are effectively changed by various In-doping concentrations. A minimum resistivity of $0.51 \times 10^{-3}$ $\Omega$ cm and carrier concentration of $5.43 \times 10^{20}$ cm$^{-3}$ with high transmittance ~80% in the range 350–800 nm were achieved for 3 wt% indium doping. The band gap value starts at 2.32 eV for the undoped film and increases with doping concentration reaching the value of 3.07 eV for 5 wt% indium doping.

## 1 Introduction

Cadmium oxide is a promising material to be used as a transparent n-type semi-conductor due to its high electrical conductivity and optical transmittance in the visible region of the solar spectrum [1]. CdO has a wide range of applications in optoelectronics, such as smart windows, phototransistors, heat mirrors and gas sensors [2, 3]. These applications are based on its structural and electro-optical properties. Many techniques have been employed to prepare pure CdO and doped CdO thin films on different substrates, such as spray pyrolysis [4], metal organic chemical vapor deposition [5, 6], reactive evaporation [7, 8], radio frequency magnetron sputtering [9], pulsed laser deposition [10, 11] and sol–gel (SG) spin coating technique [12, 13]. Among these deposition techniques, the SG spin coating technique, compared with other techniques, is simple, cost effective, and suitable for large area thin film preparation with a homogenous doping level and can produce high quality thin films of metal oxide materials. Doping is a fundamental method to control the properties of semiconductors and to obtain new taylor-made multi-functional materials.

We studied the effect of doping the CdO films with In. The (In$^{3+}$) replaces the Cd$^{2+}$ cations in the lattice sites and donates electrons acting as charge carriers and hence, is expected to be an ideal doping candidate for CdO films [14].

This work aims at a detailed investigation of the characteristics of CdO thin films that were synthesized by the SG method and annealed at 450 °C under ambient atmosphere. First we evaluate the effect of the thickness of the film on the structural, optical and electrical properties and then using

✉ I. Ben Miled
islembm2010@hotmail.fr

1. Laboratoire de Semi-conducteurs, des Nano-structures et des Technologie Avancées, Centre de Recherches et des Technologies de l'Energie, Technopole de Borj-Cédria, BP 95, 2050 Hammam-Lif, Tunisia

2. Faculté des Sciences de Bizerte, 7021 Jarzouna, Tunisia

3. Ecole Supérieure des Sciences et Technologies du Design, Université de la Manouba, P5, Den Den, Tunisia

4. Ecole Nationale d'Electronique et des Télécommunications de Sfax, Université de Sfax, BP 1163, 3018 Sfax, Tunisia

5. National Hellenic Research Foundation, Theoretical and Physical Chemistry Institute, 48 Vassileos Konstantinou Ave., 11635 Athens, Greece

the optimum thickness we report the effect of In concentration on the properties of In–CdO thin films.

## 2 Experimental details

Cadmium acetate dihydrate [Cd(CH$_3$COO)$_2$·2H$_2$O (99.5%, Sigma-Aldrich)], indium acetate [In(C$_2$H$_3$O$_2$)$_3$, (99.99%, Sigma-Aldrich)], 2-methoxyethanol [C$_3$H$_8$O$_2$; (99.8%, Sigma-Aldrich)] and mono-ethanolamine (MEA), (NH$_2$CH$_2$CH$_2$OH; 99%, Merck) were used as the precursors for the synthesis of pure and doped CdO films.

In a typical synthesis, cadmium acetate dihydrate was dissolved in 2-methoxyethanol to obtain a 0.3 M solution. The solution was stirred for 10 min at room temperature, and the temperature was ramped up to 80 °C, at that temperature MEA was added drop by drop to stabilize the solution. The ratio of MEA to cadmium(II) acetate was maintained to 1.0. The solution was stirred for 2 h at 80 °C to obtain a yellow, homogeneous and transparent solution and left to age for 24 h at room temperature. Before deposition, glass substrates were cleaned successively with acetone, ethanol, and deionized water in an ultrasonic bath. CdO thin films were deposited on the glass substrates by spin coating at room temperature, with a rate of 3500 rpm for 30 s. After each spin-coating step, the films were heated on a hot plate at 250 °C in air for 10 min to remove organic solvents. Samples with different thickness were prepared by repeating the procedure of coating and drying from one to six times. At the end all samples were annealed in air at 450 °C for 1 h. These annealing conditions give the best results mentioned in previous study [15].

A similar method was used to prepare CdO samples doped with 1, 3 and 5% In. The In acetate was added with the Cd acetate at the first step to obtain the desired analogy and the procedure of spin coating and drying was repeated four times, in order to obtain films with the optimum thickness.

The crystallographic structure of the films was studied by X-ray diffraction (XRD), using a Bruker D 8 advance, X-ray diffractometer with Cu Kα ($\lambda_{CuK\alpha} = 1.5418$ Å) radiation, for 2θ values in the range of 20–80°. The optical transmittance

of the films was measured by a UV–Vis–NIR (Lambda 950) spectrophotometer, in the wavelength range 350–800 nm. The photoluminescence (PL) spectra were recorded by a fluorescence spectrophotometer (LS 45) with an excitation wavelength of 266 nm. The thickness of the thin films was measured using a KLA Tencor Alpha-step IQ surface profilometer with an accuracy of ± 1 nm. The surface morphology of the prepared films examined by scanning electron microscopy (SEM) (Hitachi S4800 operated at 2 kV for secondary electron imaging). Electrical properties were determined using a Hall effect measurement setup (Scientific Equipments, Model: EMU.50) with a four-point probe. All measurements were carried out at room temperature.

## 3 Results and discussion

### 3.1 Dependence of the physical properties of CdO thin films on thickness

As it was expected the thickness of the films was increased with the number of the layers (Table 1).

#### 3.1.1 Structural characterizations

XRD patterns of CdO thin films grown on glass at different thicknesses are shown in Fig. 1. The XRD peaks coincide with those of cubic crystal structure according to JCPDS card No. 05-0640 [16]. For all the samples a strong orientation along the (111) and (200) is observed. Other peaks, such as (220), (311) and (222) are also observed especially at thicker samples, but their intensities are very small. Their intensities of all the peaks and especially of (111) and (200) peaks increase by increasing the thickness from 53 nm (one layer) to 246 nm (five layers) and then decrease for the thickness of 284 nm (six layers). These results are in agreement with those reported by Salunkhe [17] applying the successive ionic layer adsorption and reaction (SILAR) method. To determine the relative degree of preferential orientation among crystal planes of CdO films, the texture coefficient

**Table 1** Variation of the texture coefficient values, crystallite size (D) and band gap for various thicknesses

| Number of layers | Average thickness (nm) | Crystallite size D (111)/nm | Lattice parameter a(111)/nm | | Texture coefficient | | Eg (eV) |
|---|---|---|---|---|---|---|---|
| | | | Calculated | Standard | (111) | (200) | |
| 1 | 53 ± 03 | 31 | 4.735 | | 1.45 | 0.87 | 2.84 |
| 2 | 106 ± 08 | 35 | 4.702 | 4.695 | 1.63 | 1.04 | 2.42 |
| 3 | 142 ± 14 | 42 | 4.694 | | 1.83 | 1.21 | 2.35 |
| 4 | 211 ± 19 | 44 | 4.696 | | 1.94 | 1.26 | 2.32 |
| 5 | 246 ± 23 | 46 | 4.701 | | 1.97 | 1.37 | 2.26 |
| 6 | 284 ± 27 | 41 | 4.686 | | 1.93 | 1.29 | 2.48 |
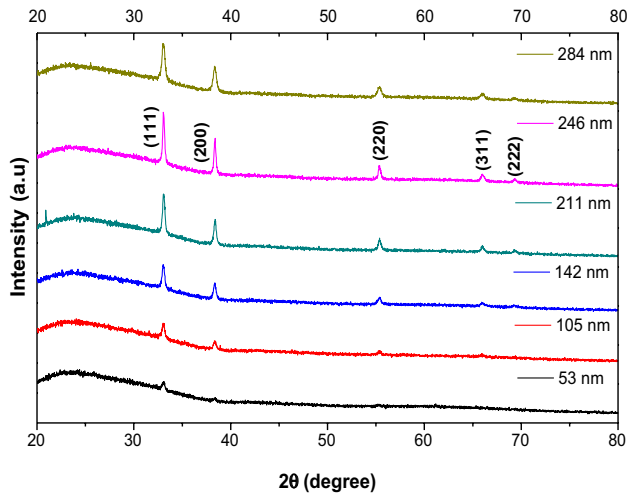
**Fig. 1** X-ray diffractograms of CdO thin films for films with different thicknesses
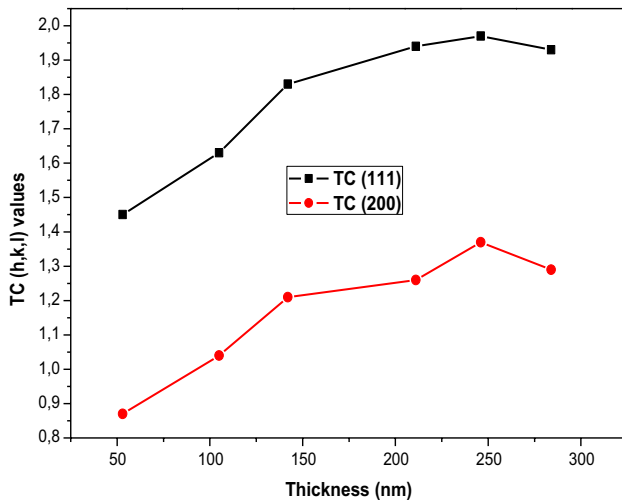


**Fig. 2** Variation of the texture coefficient for the planes (111) and (200) as a function of film thickness

TC (hkl) was calculated from the XRD data, using the well-known formula [18]:

$$TC(hkl) = \frac{I(hkl)}{I_0(hkl)} \left[ \frac{1}{n} \sum_{i=1}^{n} \frac{I(hkl)}{I_0(hkl)} \right]^{-1} \quad (1)$$

where I(h k l) is the measured intensity of X-ray reflection for the (h k l) reflection, $I_0$(h k l) is the reference diffraction pattern intensity (JCPDS card no. 05-0640), and n is the number of reflections. Values of $0 \leq T_C$ (h k l) $\leq 1$ indicate the lack of grain oriented in the corresponding direction. Figure 2 depicts the variation of TC (111) and TC (200) with film thickness. From this figure, it is clear that TC (111) has

the highest value, which increases from 1.45 to 1.97 when the film thickness increases from 53 to 246 nm, and then decreases for the sample with six layers (284 nm). TC (200) shows a similar trend like that of TC (111) but it has lower values than that of TC (111).

The lattice parameters of CdO thin films are calculated by the Nelson–Riley function [19] from the XRD patterns data using the data from all the peaks according to the Eq. (2) [20]:

$$\frac{1}{d_{hkl}^2} = \frac{h^2 + k^2 + l^2}{a^2} \quad (2)$$

The lattice parameter of the films decreased from 4.735 to 4.686 nm with increasing the thickness from 53 to 284 nm. The present obtained lattice parameter values of 4.694 and 4.696 at 142 and 211 nm respectively were close to the standard value of 4.695 nm.

The crystallite size of the film grains was calculated from the (111) peak by using Scherrer's formula [21]:

$$D = \frac{0.9\lambda}{\beta \cos \theta} \quad (3)$$

where $\beta$ is the full width at half maxima (FWHM) in radians.

The results show that the crystallite size increases from 31 to 46 nm by increasing the film thickness from 53 to 246 nm. By further increasing the thickness to 284 nm, the crystallite size decreases to 41 nm (Table 1). The decrease of the crystallite size can be attributed to the nucleation process, due to the difference in the density of nucleation centers in films with different thicknesses [22].

### 3.1.2 Effect of the thickness on the optical properties of CdO thin films

Figure 3 shows the optical transmittance and reflectance spectra of CdO films as a function of the film thickness. The average optical transmittance of the films decreased from 71 to 33% in the 350–800 nm range with increasing the film thickness from 53 to 246 nm, and the reflectivity is < 10% for all samples. The transmittance with a reflectivity of 10% for all samples, is inversely proportional to absorbance. As we notice, the transmittance of thin film decreases with increasing film thickness, it means more light is absorbed in the thick film. Further increasing the film thickness to 284 nm, decreased the transmittance of the film to 55%. This can be linked to the change in crystalline structure and with a decrease in the crystallite size of the films. It was observed that the absorption edge was shifted towards shorter wavelengths with increase of film thickness to 246 nm as a consequence of widening of the band gap [23].
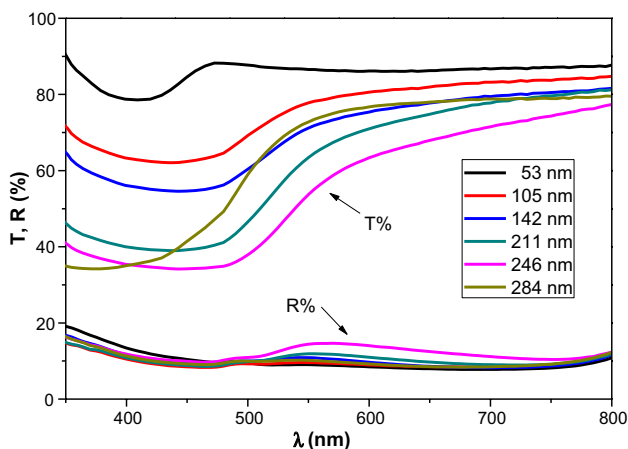
**Fig. 3** Optical transmittance and reflectance spectra for CdO for various film thicknesses

The optical band gap energy of CdO thin films was estimated by the transmittance (T) and reflectance (R) using the Tauc's method [24]:

$$\alpha h\nu = B\left(h\nu - E_g\right)^{1/2} \tag{4}$$

The absorption coefficient was calculated from the equation

$$\alpha = \frac{1}{d} \ln\left[\frac{(1-R)^2}{T}\right]$$

where d is the thickness of the sample.

We have calculated the direct optical band gap ($E_g$) by plotting $(\alpha h\nu)^2$ versus $h\nu$ and extrapolating the straight line portion of this plot to the energy axis.

The values of the optical band gap $E_g$ for all the thicknesses are given in Table 1. It is clearly observed that the value of $E_g$ decreases from 2.84 to 2.26 eV with increasing thickness from 53 to 246 nm. Further increasing the thickness to 284 nm the optical band gap energy of CdO thin films was increased to 2.48 eV. The change in energy band gap with film thickness can be understood by the decrease of structural disorder as well as increase in crystallite size in the films as observed from the microstructural analysis [25]. Anil Kumar et al. [23] also reported that the optical band gap reduces from 2.84 to 2.7 eV, with the increase of thickness of film deposited by RF magnetron sputtering technique.

The values of the optical band gap energy are in good agreement with those published by other authors [23, 25]. The optical band gap of the CdO films was changed with the increase in thickness. The results suggest that CdO thin films deposited by SG technique can be considered as a potential transparent electrode for applications in thin film solar cells [26].
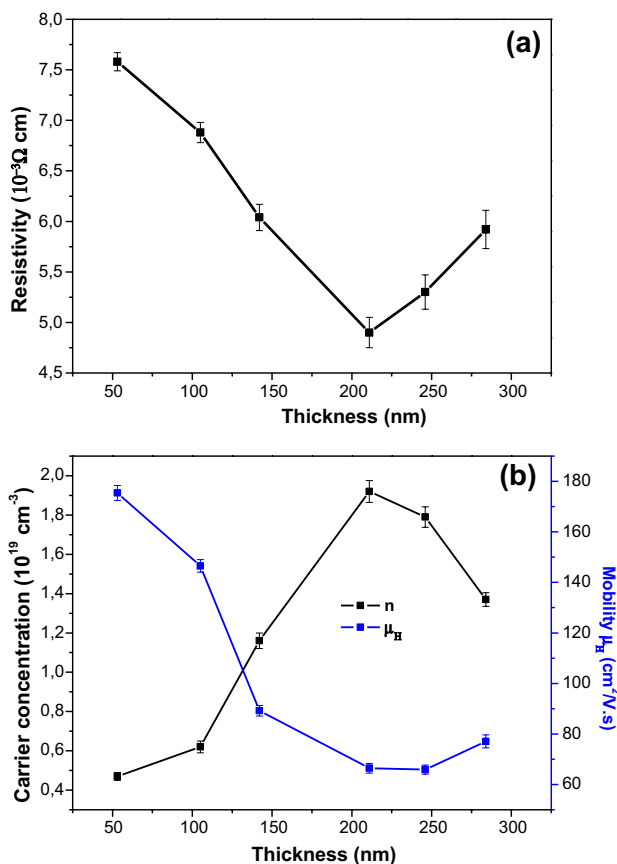


**Fig. 4** Variation of **a** resistivity ρ, **b** carrier concentration n and mobility μH of CdO films for various film thickness

### 3.1.3 Dependence of the electrical properties of CdO on thickness

The electrical properties of the films were significantly affected by film thickness. Figure 4a, b shows the electrical resistivity, the carrier concentration and the mobility of CdO films as a function of the film's thickness. The electrical resistivity of the films decreased from $7.58 \times 10^{-3}$ to $4.9 \times 10^{-3}$ Ω cm with the increase in the film thickness from 53 to 211 nm. This decrease in electrical resistivity can be attributed to the improvement of the crystalline quality of the films and the increase of grain size as revealed by XRD data. In general, the resistivity of the films can be affected by three types of electron scattering mechanisms. These are (a) isotropic background scattering (due to the combined effects of phonons and point defects), (b) scattering due to the external surface, and (c) scattering due to a distribution of planar potentials (grain boundaries) [27]. In the present work, the dependence of the resistivity of the films on the film thickness is attributed to the grain boundary scattering. The Hall mobility measurements indicate that the films show n-type conductivity. The Hall mobility of the films (Fig. 4b)

decreased from 175 to 65 cm$^2$/V s with the increase in film thickness from 53 to 211 nm. Further increasing the film thickness to 284 nm, the mobility of CdO thin films was slightly increased to 77 cm$^2$/V s. Low mobility values at higher film thicknesses were attributed to the presence of defects in the CdO films as well as scattering of these carriers at the larger grain boundaries [28].The carrier concentration of the films continuously increased from $0.47 \times 10^{19}$ to $1.92 \times 10^{19}$ cm$^{-3}$ with the increase of film thickness from 53 to 211 nm. The larger carrier concentration at higher film thicknesses indicates the presence of cadmium as an impurity in the CdO micro-crystallites which was also responsible for the reduction in the mobility. The achieved results were comparable to those of CdO films deposited by the spray pyrolysis method [29].

The CdO film composed of four layers (211 nm) presents the lowest resistivity and highest carrier concentration. Based on the obtained results, the thickness was fixed at 211 nm for the following doping experiments.

## 3.2 Effect of indium doping on structural optical and electrical properties of cadmium oxide thin films

### 3.2.1 Structural characterization

XRD patterns of the undoped CdO films and In-doped CdO films are displayed in Fig. 5, for the 450 °C annealing temperature. The films show the typical cubic crystalline structure of the cadmium oxide with five characteristic peaks assigned to the (111), (200), (220), (311) and (222) planes. For low percentages of doping, the (111) peak, observed around 33°, is the most intense and then decreases rapidly with increasing doping. Moreover, the peaks of the other
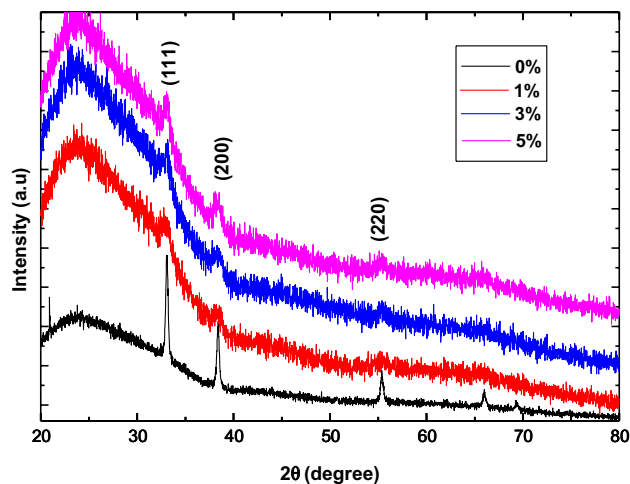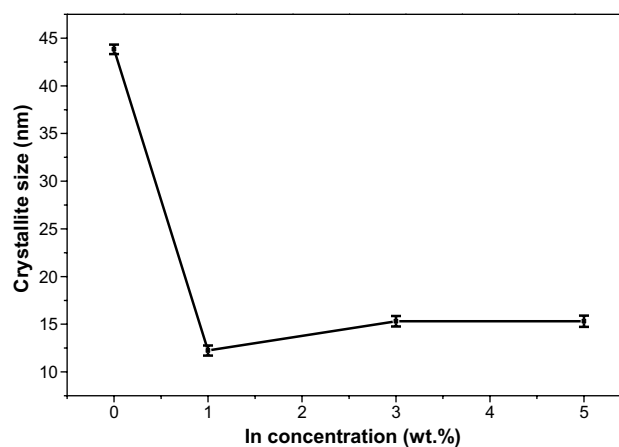
orientations disappear. This result shows that the dopant concentration greatly affects the growth kinetics of CdO thin films. The intensity of the XRD peaks declines and the half-maximum width becomes wider. It is obvious that In doping of CdO films causes the crystallinity to degrade and that the increase of In concentration the In$^{3+}$ ions inhibits the aggregating growth of CdO nanocrystals that affects the crystallization of CdO [30]. The crystallite size of the films has been estimated using the Scherrer's formula [21]. A close look at Fig. 6 suggests that the crystallite size first decreases considerably from 0 to 1% of In concentration, while for larger concentrations it slightly increases.

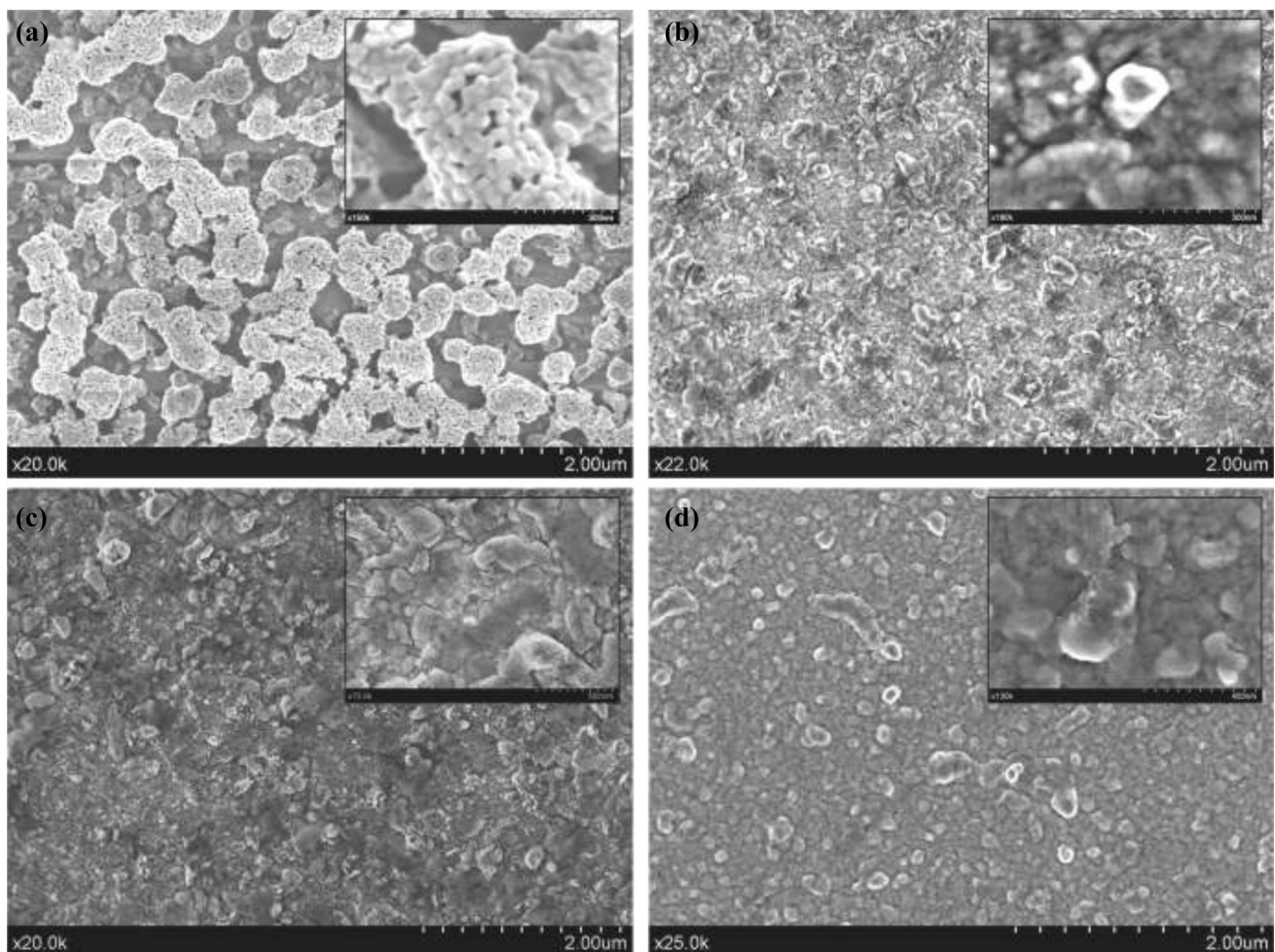### 3.2.2 Morphological properties

The surface microstructures of CdO and CdO:In thin films obtained from FE-SEM analysis are compared in Fig. 7 as a function of In concentration. The inset Fig. 4a shows grain quasi-spherical, non-uniform shapes, agglomerated and distributed over the surface of the sample. One may notice (Fig. 7a) that the CdO film is not homogenous, but seems to be granular and porous. Figure 7b–d show the surface microstructures obtained from the films deposited from 1, 3, and 5 wt% of indium concentration in the solution, respectively. Enhanced surface homogeneity was observed in all films when the proportion of In increases. Figure 7b–d reveal a mixture of microstructures on the surface, which consists of the grains with more regular shapes of spheres and elongated spherical shapes. They also show that the nanoparticles tend to agglomerate further and further as the In ratio increases.

The average grain size of the undoped and In-doped CdO films is measured from the corresponding FE-SEM microstructures and are plotted as histogram images in Fig. 8a–d. The average grain size of undoped CdO thin film is decreasing from 50 to 15 nm, following the increase in In doping



**Fig. 5** X-ray diffraction pattern of indium-doped cadmium oxide thin films for different indium concentrations



**Fig. 6** Variation of the crystallite size as a function of indium concentrations

**Fig. 7** SEM images of CdO and In-doped CdO thin films as a function of In doping: **a** 0 wt%, **b** 1 wt%, **c** 3 wt% and **d** 5 wt%

to 1 and 3 wt%, respectively. However, further increase in In doping concentration increases slightly the average grain size from 15 nm (3 wt%) to 17 nm for 5 wt% In doping. Thus, the SEM features corroborate the XRD results indicating that the particle size decreases when the In doping concentration increases.

The SEM data reveal grain sizes of the order of 15 nm, which is similar to the crystallite size measured by XRD; however, a single grain contains many crystallites. This might be due to the proper atomic concentration content. The effect of the appropriate concentration is evidenced by the spherical grains of almost the same shape and diameter [31].

### 3.2.3 Optical properties

The optical transmittance of un-doped and In–CdO films is shown in Fig. 9. It is observed that all doped films exhibited a higher transmission of about 70–80% in the range of 500–800 nm. The transparency of the CdO films increases

with the increase in In concentration from 0 to 1%. Furthermore a slight decrease in the transparency is observed for 3 and 5 wt% of In. The enhanced optical transmittance of CdO films may be due to the change in the crystallite size on In-doping up to 1 wt%. The slight decrease in transmittance above 1 wt% of In-doping may be due to the incorporation of more In in the lattice sites and in the interstitial positions, thus leading to increase in the absorption. Figure 9 also shows the reflectance spectra of In–CdO films. As seen in Fig. 9, there is an orderly increase in reflectance values of the films with increasing In doping. Especially, low reflectance value of CdO thin films makes this film a promising material as a window for photovoltaic applications.

The energy band gap was estimated from the plot of $(\alpha h\nu)^2$ versus $(h\nu)$, where $\alpha$ is the absorption coefficient and $h\nu$ is the photon energy. The band gap energies of the films were determined by the extrapolation of the linear regions on the energy axis $(h\nu)$. It is clear from Fig. 10 that the band gap value increases by increasing the In concentration in the CdO film. This increase in optical band gap was
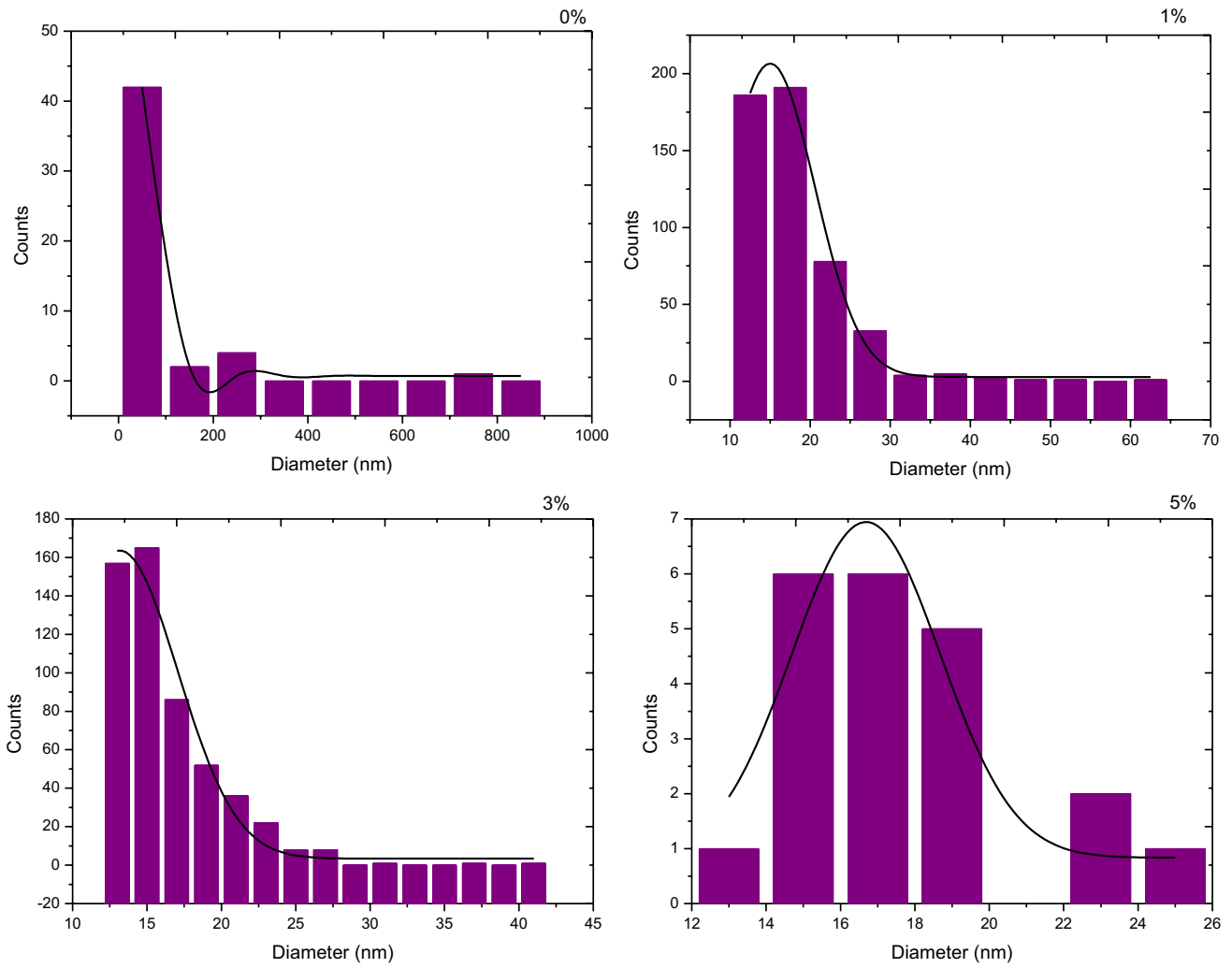
**Fig. 8** Histogram image for measuring average grain size: **a** CdO, **b** 1 wt % In, **c** 3 wt % In, and **d** 5 wt % In doped CdO thin films
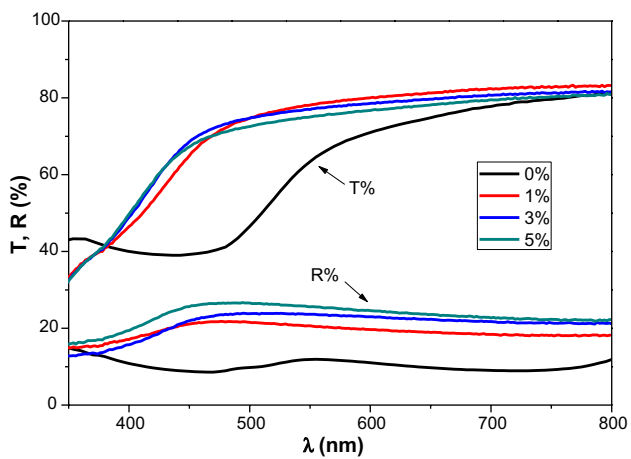


**Fig. 9** Optical transmittance and reflectance spectra for In–CdO with different In concentrations
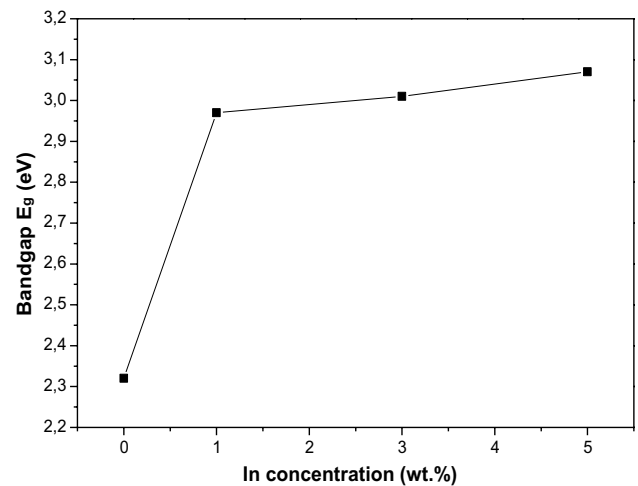


**Fig. 10** Variation of energy band gap as a function of In concentration

also observed for Ni-doped CdO thin films prepared by Yakuphanoglu [32] and for Al-doped CdO thin films prepared by the spray pyrolysis method [33]. The band gap value for CdO film without doping is 2.32 eV (four layers), while the doping of 5 wt% indium results in an increase of band gap to 3.07 eV. The blue shift of the band gap energy may be attributed to the increase in carrier concentration. Table 2 shows the optical band gap of In-doped CdO thin films with different preparation techniques. With increase in carrier concentration, filling of the lowest states in the conduction band takes place, a phenomenon known as the Burstein–Moss effect [34]. The present 5 wt% In–CdO film shows a band gap of 3.07 eV, which is similar to the value of 3.0 eV reported for Sn doped CdO film [32]. This blue shift of band gap energy, combined with the evident decrease of resistivity (see Sect. 3.2.5 below), makes In–CdO films to be a potential candidate for window layer in solar cells and other optoelectronic applications.

### 3.2.4 Photoluminescence study

Figure 11 shows the room temperature PL spectra of undoped CdO and In–CdO thin films with an excitation wavelength of 266 nm. The PL peaks of In–CdO thin films showed broad emission peaks in the near UV and blue-green spectral region. Five bands are observed after doping, at 340, 428, 441, 475 and 528 nm.

The UV emission with a peak at 340 nm exists for all dopant concentrations but does not exist for pure (undoped) CdO films; this can be attributed to the oxygen vacancies of In [39]. The peak at 428 nm is due to an exciton bound to a donor level [39]. The 441 nm emission band which emerges for higher concentration (5 wt%) may be due to the oxygen defects ($V_{In–O}$) bounded with In–O [40]. The peaks at 475 nm (blue emission) and 528 nm (green emission) can be attributed to deep-level or trap-state emission, corresponding to interstitial cadmium and oxygen vacancies respectively [41, 42]. Oxygen vacancies play an important role in CdO nanostructures [43]. It is remarkable that the broad emission band centered at 475 nm decreases after doping at 1 and 3 wt% In concentration and then disappear with increasing In concentration at 5 wt%.
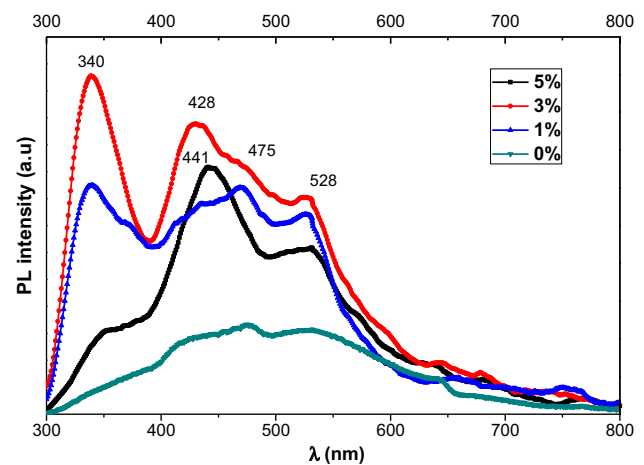
**Fig. 11** Photoluminescence spectra undoped and In–CdO thin films

### 3.2.5 Electrical properties

Figure 12a, b illustrates the variation in resistivity (ρ), the carrier concentrations (n), and Hall mobility ($\mu_H$) as a function of In concentration in In–CdO thin films. It can be seen that the electrical parameters are strongly affected by In doping in the CdO films. As the In concentration increases from 0 to 5 wt%, the resistivity decreases considerably from $4.9 \times 10^{-3}$ Ω cm to the minimum value of $0.51 \times 10^{-3}$ Ω cm (Fig. 12a). An indium doping concentration of 3 wt% has been the optimum concentration for the preparation of In–CdO films (Fig. 12a) for electrical applications.

Resistivity is proportional to the reciprocal product of carrier concentration n and mobility $\mu_H$. The observed decrease of the resistivity is due to an increase of the carrier concentration. The undoped CdO thin film exhibits a carrier concentration of $1.92 \times 10^{19}$ cm$^{-3}$ (Fig. 12b). This value increases with In doping and the maximum value of $5.43 \times 10^{20}$ cm$^{-3}$ was obtained for 3 wt%. Table 2 shows the electrical properties of the present In–CdO films compared with doped and undoped CdO films fabricated by different methods. The higher value of carrier concentration n may originate from the replacement of $Cd^{2+}$ ions by $In^{3+}$ ions in the CdO lattice [44]. The further slight decrease of n may indicate a limit of solubility of In in the CdO matrix. On the

**Table 2** A summary of electrical and optical properties of undoped and In doped CdO films by various methods

| Materials | ρ (Ωm) | n ($10^{20}$ cm$^{-3}$) | μ (cm$^2$/V s) | Eg (eV) | Methods | References |
|---|---|---|---|---|---|---|
| CdO | $4.9 \times 10^{-3}$ | 0.19 | 66.83 | 2.32 | Present work | Present work |
| CdO:In (3 wt%) | $5.14 \times 10^{-4}$ | 5.43 | 22.43 | 3.07 | Present work | Present work |
| CdO | $2.03 \times 10^{-3}$ | 1.96 | 12 | 2.61 | Spray pyrolysis | [35] |
| CdO:In (3 wt%) | $3.36 \times 10^{-3}$ | – | – | 2.62 | Spray pyrolysis | [36] |
| CdO:In (5 wt%) | $10^{-3}$ | 2.8 | 30 | 3.1 | SG | [37] |
| CdO:In (3.9 wt%) | $5.95 \times 10^{-5}$ | 10.21 | 96 | 2.97 | PLD | [38] |
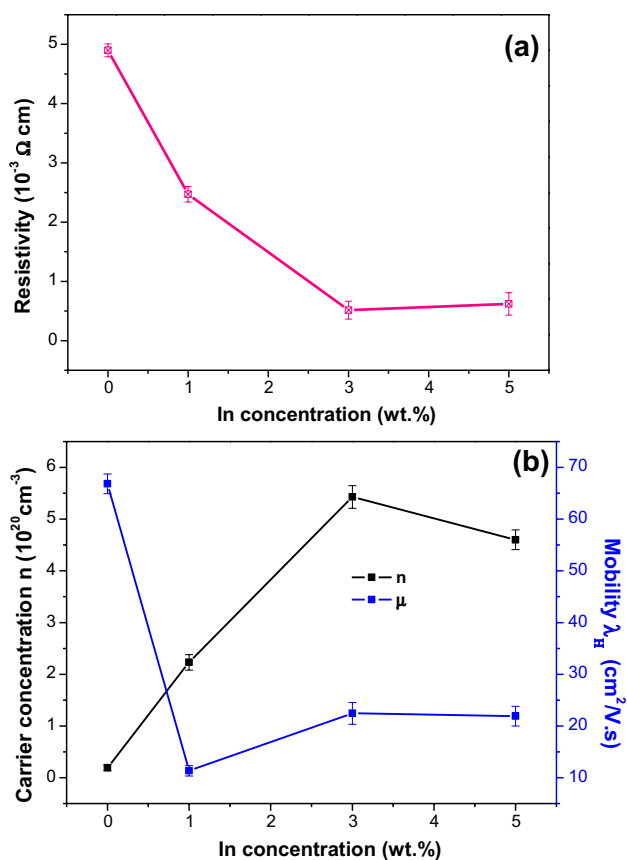
**Fig. 12** Variation of **a** resistivity ρ, **b** carrier concentration n and mobility μH of CdO

other hand, the mobility which initially was 66.83 cm²/V s for undoped CdO film, decreases fast with increasing indium doping concentration from 0 to 1 wt% and then it increases slightly to 22.43 cm²/V s for 3 wt%. The decrease in mobility is due to the loss of crystallinity [42], (see also Fig. 6), because μ is sensitive to grain boundaries scattering. Therefore, In–CdO thin films, grown via SG spin coating technique, may be an excellent candidate for future optoelectronic devices.

## 4 Conclusions

The structural, optical, and electrical properties of CdO thin films, deposited by a SG spin coating technique, were investigated as a function of the film thickness. Subsequently, the effect of In-doping concentration on the structural, optical and electrical properties of In–CdO films, for a thickness of 211 nm, was analyzed. The polycrystalline In–CdO films were confirmed to have cubic crystal structure with no evidence of $In_2O_3$ or other mixed phases. In–CdO films exhibited high optical transmittance with increased band gap value in respect to the undoped one. The band gap value of

2.32 eV for the undoped CdO increased and reached a value of 3.07 eV for 5 wt% In-doping, due to the Moss–Burstein effect. A minimum resistivity of $0.51 \times 10^{-3}$ Ω cm with maximum carrier concentration of $5.43 \times 10^{20}$ cm$^{-3}$ was achieved at the In-doping concentration of 3 wt%. These results indicate the n-type In–CdO films as an ideal candidate for transparent electrodes in optoelectronic devices.

## References

1. R. Ferro, J.A. Rodríguez, Sol. Energy Mater. Sol. Cells **64**, 363–370 (2000)
2. R. Chandiramouli, B.G. Jeyaprakash, Solid State Sci. **16**, 102–110 (2013)
3. R.H. Bari, S.B. Patil, Int. Lett. Chem. Phys. Astron. **18**, 31–46 (2014)
4. I. Akyuz, S. Kose, E. Ketenci, V. Bilgin, F. Ayata, J. Alloys Compd. **509**, 1947–1952 (2011)
5. A.W. Metz, J.R. Ireland, J.G. Zheng, R.P.S.M. Lobo, Y. Yangm, J. Li, C.L. Stern, V.P. Dravid, N. Bontemps, C.R. Kannewurf, K.R. Poeppelmeier, T.J. Marks, J. Am. Chem. Soc. **126**, 8477–8492 (2004)
6. S. Jin, Y. Yang, J.E. Medvedeva, J.R. Ireland, A.W. Metz, J. Ni, C.R. Kannewurf, A.J. Freeman, T.J. Marks, J. Am. Chem. Soc. **126**, 13787–13793 (2004)
7. Y. Yang, S. Jin, J.E. Medvedeva, J.R. Ireland, A.W. Metz, J. Ni, M.C. Hersam, A.J. Freeman, T.J. Marks, J. Am. Chem. Soc. **127**, 8796–8804 (2005)
8. A.A. Dakhel, F.Z. Henari, Cryst. Res. Technol. **38**, 979–985 (2003)
9. T.K. Subramanyam, S. Uthanna, B. Srinivasulu Naidu, Appl. Surf. Sci. **169**, 529–534 (2001)
10. R.K. Gupta, K. Ghosh, R. Patel, S.R. Mishra, P.K. Kahol, Mater. Lett. **62**, 3373–3375 (2008)
11. R.K. Gupta, K. Ghosh, R. Patel, S.R. Mishra, P.K. Kahol, Curr. Appl. Phys. **9**, 673–677 (2009)
12. J. Santos Cruz, G. Torres Delgado, R. Castanedo Perez, C.I. Zuniga Romero, O. Zelaya Angel, Thin Solid Films **515**, 5381–5385 (2007)
13. P.K. Ghosh, R. Maity, K.K. Chattopadhyay, Sol. Energy Mater. Sol. Cells **81**, 279–289 (2004)
14. A. Wang, J.R. Bancock, N.L. Edleman, A.W. Metz, M.A. Lane, R. Asahi, V.P. Dravid, C.R. Kannewurf, A.J. Freeman, T.J. Marks, Proc. Natl. Acad. Sci. USA **98**, 7113–7116 (2001)
15. I. Ben Miled, M. Jlassi, I. Sta, M. Dhaouadi, M. Hajji, G. Mousdis, M. Kompitsas, H. Ezzaouia, J. Sol-Gel Sci. Technol. **83**, 259–267 (2017)
16. JCPDS—International Centre for Diffraction Data (1997) CardNo. 05-0640
17. R.R. Salunkhe, C.D. Lokhande, Sens. Actuators B **129B**, 345–351 (2008)
18. C.S. Barret, T.B. Massalski, Structure of Metals (Pergamon Press, Oxford, 1980)
19. J.B. Nelson, D.P. Riley, Proc. Phys. Soc. London **57**, 160 (1945)
20. J. S. Blakemore, Solid state phys. **12**, 506 (1985)
21. B.D. Cullity, S.R. Stock, Elements of X-ray diffraction, 3rd edn. (Prentice Hall, NJ, 2001)
22. I. Sta, M. Jlassi, M. Hajji, M.F. Boujmil, R. Jerbi, M. Kandyla, M. Kompitsas, H. Ezzaouia, J. Sol-Gel Sci. Technol. **72**, 421–427 (2014)
23. G. Anil Kumar, M.V. Ramana Reddy, K. Narasimha Reddy, Solid State Phys. AIP Conf. Proc. **1591**, 1003–1005 (2014)

24. J. Tauc, R. Grigorovici, A. Vancu, Phys. Status Solid B **15**, 627–637 (1966)
25. V.P. Geetha Vani, M. Vasudeva Reddy, K.T. Ramakrishna Reddy, J. Phys. Condens. Matter. Article ID 142029 (2013)
26. S. Aydemir, S. Köse, M.S. Kilickaya, V. Özkan, Superlattices Microstruct. **71**, 72–81 (2014)
27. A.F. Mayadas, M. Shatzkes, Phys. Rev. B **1**, 1382–1389 (1970)
28. H.U. Hubermier, Thin Solid Films **80**, 157–160 (1981)
29. L.C.S. Murthy, K.S.R.K. Rao, Bull. Mater. Sci. **22**, 953–957 (1999)
30. M. Jlassi, I. Sta, M. Hajji, H. Ezzaouia, Appl. Surf. Sci. **301**, 216–224 (2014)
31. R.J. Deokate, S.V. Salunkhe, B.S. Pawar, K.Y. Rajpure, A.V. Moholkar, J.H. Kim, S.M. Pawar, K.Y. Rajpure, A.V. Moholkar, J.H. Kim, J. Alloys Compd. **496**, 357–363 (2010)
32. F. Dagdelen, Z. Serbetci, R.K. Gupta, F. Yakuphanoglu, Mater. Lett. **80**, 127–130 (2012)
33. M. Thirumoorthi, J.T.J.Prakash, J. Asian. Ceramic. Soc. **4**, 39–45 (2016)
34. E. Burstein, Phys. Rev. **93**, 632–701 (1954)
35. K. Sankarasubramanian, P. Soundarrajan, K. Sethuraman, K. Ramamurthi, Mater. Sci. Semicond. Process. **40**, 879–884 (2015)
36. S. Kose, F. Atay, V. Bilgin, I. Akyuz, Int. J. Hydrogen Energy **34**, 5260–5266 (2009)
37. M.A. Flores, R. Castanedo, G. Tornes, O. Zelaya, Sol. Energy Mater. Sol. Cells **93**, 28–32 (2009)
38. B.J. Zheng, J.L. Lian, L. Zhao, Q. Jiang, Appl. Surf. Sci. **256**, 2910–2914 (2010)
39. Z.R. Khan, M.S. Khan, M. Zulfequar, M. Shahid Khan, J. Mater. Sci. **2**, 340–345 (2011)
40. S. Kundu, P.K. Biswas, Chem. Phys. Lett. **414**, 107–110 (2005)
41. F.E. Ghodsi, H. Absalan, Acta Phys. **118**, 659–663 (2010)
42. W.-N. Wang, W. Widiyastuti, T. Ogi, I.W. Lenggoro, K. Okuyama, Chem. Mater. **19** 1723–1730 (2007)
43. B. Goswami, A. Choudhury, J. Exp. Nanosci. **10**, 900–910 (2014)
44. R. Kumaravel, K. Ramamurthi, V. Krishnakumar, J. Phys. Chem. Solids **71**, 1545–1549 (2010)